

Design and Evaluation of a Novel Low Acoustic Impedance-Based PZT Transducer for Detecting the Near-Surface Defects

Ali Mohammadabadi^{1,2}, Roberto Dugnani^{1,*}

¹Department of Mechanical Engineering, University of Michigan - Shanghai Jiao Tong University Joint Institute, Shanghai, China

²Department of Mechanical Engineering, University of Maryland, Baltimore County, MD 21250 USA

Received 10 February 2019; received in revised form 10 March 2019; accepted 10 April 2019

Abstract

Near-surface defects are one of the most common types of damage occurring in polymer composite materials. Conventional Non-Destructive Testing (NDT) techniques, especially ultrasonic testing, are not always suitable for detecting these types of defect, especially in thin plates. The proposed NDT method in this article employs Low Acoustic Impedance (LAI) characterization. The novelty of LAI technique lies in the transverse resonating of Lead-Zirconate-Titanate (PZT) transducer which shows significant lower effective acoustic impedance compared to thickness - extension mode. The LAI technique eliminates the need for the matching layers and reduces the manufacturing cost consequently. Briefly, the analytical model has been introduced and the fabrication procedure has been discussed in detail. The setup has been evaluated both numerically and experimentally to detect a debonding. The results proved the ability of LAI technique in the detection of defects and, moreover, the approximate geometry of the affected region as well.

Keywords: non-destructive testing, low acoustic impedance, self-sensing transducer

1. Introduction

In this article, we introduce a novel technique which does not require broadband/high-voltage signals in the detection of near-surface damages. We were interested to develop an inexpensive and simple technique for a qualitative evaluation of materials with low acoustic impedance. These materials include a wide range of natural materials like wood and biological organs to advanced materials such as polymer composites. Composites are getting more attention due to their noticeable strength versus their light weight. Their defects like debonding, porosities and delamination may lead to the severe failure of structures. Similarly, wooden structures are still popular, and their natural or operational defects are always critical to the life of the structures. The detailed evaluation and application of our proposed technique for composite and wooden structures as the target groups will be discussed in separate articles.

Traditional and more advanced Non-Destructive Evaluation (NDE) techniques provide detailed quantitative information about damages and abnormalities in structures. Different aspects of structural NDEs were discussed by [1, 2]. On the other hand, new technologies helped to increase the accuracy and viability of these techniques. For example, [3] discussed the applications of artificial intelligence in the SHM and NDE. As a general insight to the future of the NDE, [4] discussed the next generation of smart sensing for the NDE applications. PZT transducers are often used in Ultrasonic Testing (UT). However, they have been used for other applications as well. [5, 6] investigated the energy harvesting by PZTs which can be used to

* Corresponding author. E-mail address: roberto.dugnani@sjtu.edu.cn

Tel: +86-21-34206765 Ext. 5181

self-charging in SHM and wireless monitoring applications. In the process of health monitoring, transducers are bonded or embedded to the surface of the specimen to excite the host structure with a range of frequency and monitor the changes of mechanical impedances [7-9]. Ultrasonic NDE has a limitation in the detection of near-surface defects such as delamination of plies which was discussed by [10, 11]. This limitation occurs because the normal pulse-echo ultrasonic technique has difficulty in resolving the echo of near-surface defects. The echo lies within a wavelength of the transmitted ultrasonic pulse. Dugnani [12] discussed that unlike the ultrasonic technique, the impedance-based technique can detect near-surface defects. Typically, few different frequencies are used in ultrasonic methods, therefore, the acoustic behavior and mechanical properties of the specimen should be known well enough to choose the right frequency which could be correlated with mechanical properties of the specimen. The impedance-based method does not have this limitation and it can sweep a range of frequencies. In addition, ultrasonic methods rely on pulsed waves which require a broad-band actuator, whereas, Impedance often relies on narrow-band signals and hence simplifying the signal analysis and the cost associated with the controlling circuit. Generally, the ultrasonic technique needs an experienced operator to run, collect and interpret data, but impedance technique has a simple setup and easy data interpretation. However, impedance technique versus the wave propagation method has been utilized in SHM widely due to its simplicity, qualitative results, and autonomous capability, which the ultrasonic wave propagation method does not have these features typically [13-15].

Dugnani [12, 16] discussed that the internal defects such as delamination, debonding, cracks and corrosion change the measured mechanical impedances. The impedance-based technique is qualitative; therefore, it needs a reference base to compare the results. This technique requires a PZT an actuator and a sensor but using a single PZT transducer as self-sensing actuator shows several advantages. The cost range of UT devices depends on testing equipment and the frequency range of the transducers. The precise and detailed evaluation of structures needs heavy and costly data processing. Because of the large volume of collected data, traditional techniques usually require off-line data processing which increases the evaluation time and cost as well. However, just checking the cost of regular devices from reliable manufacturers, [17] shows that they are relatively expensive compared to the proposed low-cost LAI setup in this article which will be discussed later. Many ordinary NDE situations do not need very detailed evaluation, and just a qualitative on-line health monitoring of structure would be enough [18]. In these cases, the inspectors are just interested to know if there is any change in the conditions of the structure versus the healthy reference bases. Since the demands for the routine inspection of structures based on the fast-qualitative is increasing, the needs for the online, cheap and real-time NDE techniques are growing.

Required hardware and software of impedance-based technique has been discussed already by [12, 19]. The novelty of this study is the design and making a portable self-sensing PZT system which uses the radial resonance mode of the PZT transducer. Regarding the self-sensing PZT, [12] discussed the theory and technical aspects of the terms entirely. Briefly, various applications of a self-sensing feature of PZT transducers have been introduced in earlier studies. For instance, [20] employed the technique to characterize the plaques in human arteries by acoustic impedance or Mohammadabadi [21] used the technique for damage detection in wooden products. [22] used self-sensing PZT to identify the fatigue crack from linear (alpha) and nonlinear (beta) ultrasonic recorded parameters. [23] discussed the application of self-sensing PZT technique for composite materials and they could successfully detect the cracks caused by an impact in the polymer composite plates. Self-sensing transducers have been employed in vibration control of flexible structures, while optimized controller design is an important challenge. For instance, an earlier study by [24] showed that the vibration of the cantilever beam can be controlled using a self-sensing actuator. The cantilever actuator by a self-sensing transducer was demonstrated and validated by [25].

2. LAI Transducer Working Principles

2.1. PZT working principle

The mechanical impedance is the ratio of the applied force to the resulting velocity and the electrical impedance is the ratio of applied voltage and the resulting current. The coupling property of piezoelectric materials provides this ability to

extract the mechanical impedance information from electrical impedance measurement. Briefly, a constant voltage over a pre-set frequency's range is provided to the PZT transducer by the analyzer. The magnitude and phase of the steady-state current drawn of the PZT transducer are recorded and the real and the imaginary parts of the electrical admittance, Y (the reciprocal of the electrical impedance) is computed. In general, the capacitive portion of the electrical signal shows a normal gradual change in the impedance curve, but the structural interaction creates sharp peaks that represent the structural resonance. In other words, the defects cause direct changes in the structural stiffness and/or damping. These changes modify the local dynamic characteristics and appear in the recorded impedance. The electromechanical 1D model of coupled PZT, the structure is shown in Fig. 1(a).

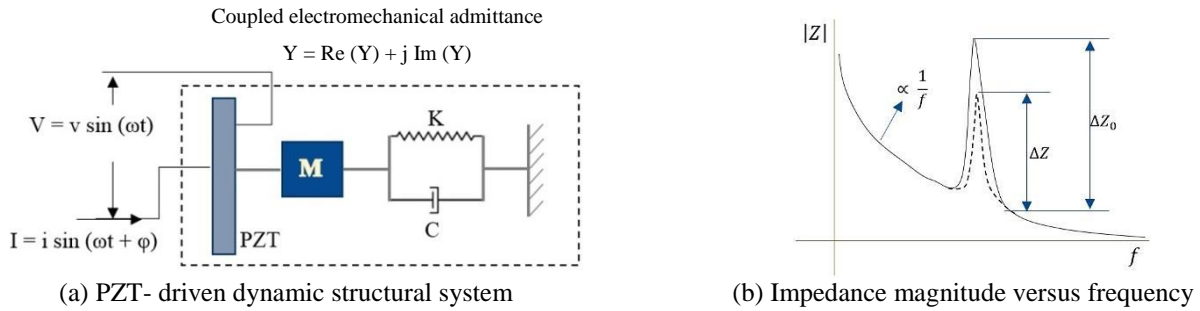


Fig. 1 Theory of an impedance-based system

In the left figure, K is the spring constant, C is the damping constant, ω is the angular frequency, ϕ is the phase and Y is the admittance. In addition, V and I are voltage and current respectively. The right figure shows the impedance magnitude versus the frequency. In this figure, ΔZ refers to the portion of the measured impedances corresponding to PZT-structure's interaction; ΔZ_0 refers to the measured impedance for the unloaded PZT transducer (i.e., in the air).

The real part of measured impedance called resistance (R) and an imaginary part called reactance (X). The sensor's capacitance for the frequency, f can be written as:

$$C_s = \frac{1}{-\omega X} = \frac{1}{-2\pi \cdot f \cdot X} \quad (1)$$

It is convenient to ignore the capacitive part of measured impedance when we study the PZT-structure's interaction because the aim of the measurement is to detect changes caused by defects and abnormalities which appear in the real part of the impedance. The impedance corresponding to the resonance peak of the PZT-structure's interaction subtracted from the capacitance of the sensor is referred to as ΔZ in this research, as in Fig. 1(b). The schematic illustration of ΔZ in Fig. 1(b) will be used as an evaluation meter to detect changes in the structure's response to the excitation by the PZT transducer.

2.2. Radial resonance mode

Traditionally acoustic transducers are designed to operate at frequencies corresponding to the thickness mode's resonant frequency. Nonetheless, at the operational frequency, these transducers display high characteristic acoustic impedances. In the case of piezoelectric ceramic transducers, the characteristic impedance of the material is at least one order of magnitude higher than the acoustic impedance of fluids and polymeric matrix materials. To improve energy transmission, transducers are often supported by various intermediate layers designed to reduce effective mechanical impedance. These layers reduce the impedance mismatching which is a negative phenomenon.

The mechanical impedance of a transducer which is transmitting in an orthogonal direction to the resonant direction is considerably lower than the characteristic impedance of the material itself. The effective mechanical impedance of an actuator coupled in a direction transverse to the resonating frequency can be significantly less than its thickness mode counterpart and it could be tuned by changing the aspect ratio between the actuator's thickness and its diameter, discussed by [16, 26, 27].

Admittance, Y , is the reciprocal of impedance. Therefore, we may use both terms in the study. Fig. 2 shows a plot of the real part of the admittance, Y , as a function of the media's acoustic impedance for a transducer resonated in the thickness mode and for a transducer resonated in the radial mode. The plot was created by numerical simulation and obtained by placing a sensor in contact with a semi-infinite surface with a given characteristic impedance. The dimensions of the transducers were chosen so that the resonant frequency of both transducers was the same for the thickness and radial modes. The minimum value for the real part of the admittance in each curve corresponds to the maximum energy dissipated by the transducer, and hence the maximum energy transferred into the structure. As expected, the maximum energy transferred for the transducer resonated in the radial mode occurs for much lower values of the medium's acoustic impedance compared to the one resonated in the thickness mode. This indicates that transducer resonated radially transfers energy more effectively than the transducer resonated in its thickness mode. Fig. 2 shows the real part of admittance divided by cross-section area for radial ($D/H = 12.5$) and thickness ($H/D = 2.7$) resonance modes, simulated by Finite Element Method; H : height and D : diameter.

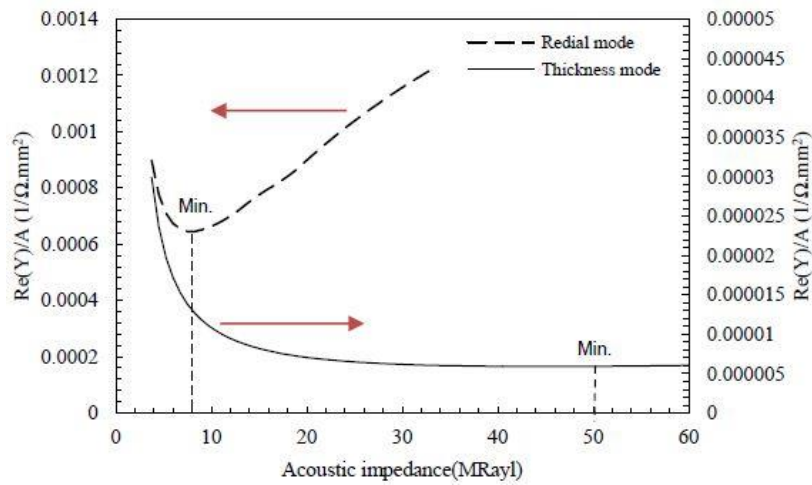


Fig. 2 Real part of admittance for the radial and thickness modes

2.3. LAI analytical principle

Electromechanical coupling property of PZT is the core of impedance-based technique. The coupling property of PZT describes the generation of electric charge in the material when subjected to mechanical stress; vice versa the converse effect describes the generation of mechanical strain when an electric field is imposed. Linear piezoelectric materials show a linear relation between mechanical and electrical variables. [28] showed that the linear relation for 1D configuration can be described as the following:

$$S_2 = \bar{s}_{22}^E T_2 + d_{32} E \tag{2}$$

$$D_3 = d_{32} T_2 + \bar{\epsilon}_{33}^T E \tag{3}$$

where S_2 is a mechanical strain, \bar{s}_{22}^E is the complex compliance at zero electric field, T_2 is the mechanical stress, d_{32} is the piezoelectric constant, E is the applied electric field, D_3 is the electric displacement and $\bar{\epsilon}_{33}^T$ is the complex dielectric constant of PZT at zero stress. The 1D governing vibration equation of PZT transducer in the longitudinal direction has been introduced as following [29]

$$\bar{Y}_{22}^E \frac{\partial^2 v}{\partial y^2} = \rho \frac{\partial^2 v}{\partial t^2} \tag{4}$$

where ρ is the density, v is the displacement in y -direction and \bar{Y}_{22}^E is the complex modulus of PZT at zero electric field. Using the separation method for solving Eq. (4) will lead to a general solution as following:

$$v = (A \sin ky + B \cos ky)e^{i\omega t} \quad (5)$$

$$k = \omega \sqrt{\frac{\rho}{\bar{Y}_{22}^E}} \quad (6)$$

where k is the wave number and ω is the angular frequency in Eq. (6). After applying the proper boundary conditions in Eq. (5) and substituting in previous equations, [28] used the definitions of current and the electrical admittance to introduce the Eq. (7) which correlates the measured electromechanical admittance, Y , (inverse of impedance) to the mechanical impedance of the structure, Z as a function of frequency for a rectangular sample transducer with the dimension of $2l_a * w_a * h_a$ as following:

$$Y = 2\omega j \frac{w_a l_a}{h_a} \times \left[\left(\bar{\epsilon}_{33}^T - d_{32}^2 \bar{Y}_{22}^E \right) + \left(\frac{z_a}{z + z_a} \right) d_{32}^2 \bar{Y}_{22}^E \left(\frac{\tan kl_a}{kl_a} \right) \right] \quad (7)$$

where l_a is the axial length, w_a is the width, h_a is the height of the transducer and Z_a is the mechanical impedance of the transducer in the direction of resonance. As [28] explained in detail, Eq. (7) can be simplified furthermore which is not the subject of this study. Eq. (7) can be used for a regular thickness mode, but we employed the modified version for the radial mode where the admittance equation for a transverse load, Z^* , was modified by [12] as follows:

$$\bar{Y} = i\omega \frac{w_a l_a}{h_a} \bar{\epsilon}_{33}^T \frac{\pi}{2} \frac{\sin(\bar{k}_2 l_a)}{\bar{k}_2 l_a} \times \left[1 + \frac{d_{33}^2 \bar{Y}_{33}^E}{\bar{\epsilon}_{33}^T} \left(\frac{z_a}{z^* + z_a} \right) \frac{z^*}{z_a} \right] \quad (8)$$

As we mentioned, the aim of this study is employing the concept of self-sensing PZT on the radial mode and making a portable and easy-to-use device for the qualitative NDE applications. Therefore, we did not focus on the analytical part and the corresponding equations. The details of Eqs. (7-8) can be obtained from the references. However, the optimization techniques such as norm based techniques [30] will help to improve the parameters of self-sensing coupling. [31] reviewed the optimization criteria for the optimal placement of the PZT transducers. In a different study, [32] used optimization methods on the impedance curves to find the optimum material properties.

3. Transducer Design

As we discussed, the conventional NDE devices are expensive and complicated for the regular qualitative structural health monitoring. Therefore, we are proposing a low-cost and easy to use LAI setup for the detection of defects in LAI materials. Briefly, the system setup includes a PZT transducer, an evaluation board, and the software. For this study, we are using a regular PZT transducer provided by APC International Ltd (American Piezo Ceramics Ltd). The type of PZT transducer is APC850 (PZT-5A) and the price of the piezo disk with an approximate diameter of 10 mm and a thickness of 3.7 mm is very cheap. The AD 5933 evaluation board has been supplied by Analog Devices Co which is also cheap. The accessories including coaxial cable, BNC connectors, frame's fabrication, etc. do not cost much. Therefore, the total approximate cost of LAI setup is very low and does not exceed than \$150 which is much cheaper than the conventional NDE devices. The software is free and easy to use, and the entire of the system is portable and user-friendly. The proposed LAI setup is shown schematically in Fig. 3. This Setup includes the PZT transducer, impedance evaluation board (AD5933) and the install software on a PC. We will show that when the PZT transducer arrives on a defect or abnormality in the testing specimen, the measured impedance will change compared to the healthy part of the specimen and this can be used as an indicator of the abnormality in the location. We will later show that this simple setup will detect the approximate geometry of the defect as well.

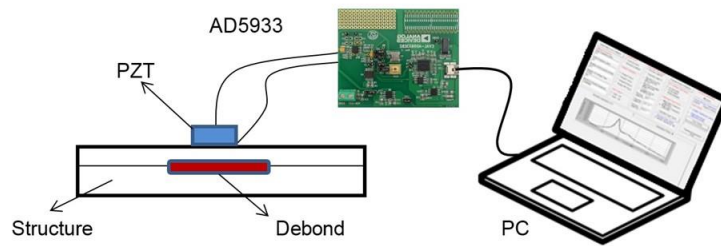
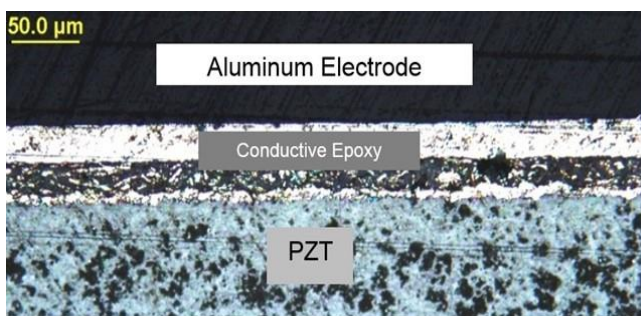


Fig. 3 LAI schematic test set-up

3.1. Transducer manufacturing

PZT-5A (American Piezo Ceramics, APC850) piezoelectric sensor with a diameter of 10 mm and a thickness of 3.7 mm was used in this test setup. This size and type of PZT were chosen to meet the required radial and planar resonance frequencies supported by the evaluation board and also, its low cost and market validity for the detection of small size defects. To ensure the flatness on the sensing side of the transducer, in the first test prototype, a flat aluminum foil was glued to the PZT sensor by means of conductive epoxy glue on the sensing side. A second wire was soldered on the opposite side. The first prototypes of the PZT transducer didn't have any frame and wires were connected to the electrode terminals by conductive epoxy directly. Microscope imaging of the cross-sectioned transducer, Fig. 4(a) indicates that both the aluminum foil electrode and the silver conductive epoxy's thicknesses are approximately 30 μm thick. The cross-section of the electrode area shows the aluminum electrode (top), silver epoxy, the tin electrode (not labeled), and PZT substrate (bottom).

The first transducer prototypes are shown in Fig. 4(b) as well. In these early prototypes, the cables were connected to PZT terminals by conductive epoxy. They could be soldered as well, but PZT is sensitive to high temperature, therefore the soldering process must be fast and under controlled temperature. The PZT transducer needs to be held consistently on the specimen for every location's impedance measurement. However, holding this small PZT transducer on the surface of the specimen was not easy. On another hand, the wires were connected to electrode terminals by conductive epoxy which was fragile, and the wires have been disconnected several times during the experiments because of the unprotected electrode terminals. The solution was covering the traces and designing a frame. Therefore, a frame was designed and fabricated for easy handling of PZT transducer and protection of electrode terminals against the physical damages like sudden pulling or twisting.



(a) Cross-section of the transducer



(b) Prototypes of PZT transducer

Fig. 4 LAI PZT transducer

Several prototypes have been designed and fabricated to improve durability and effective measurements. The design goal was developing a stable and easy-handled LAI device, which could be operated without external interference in the radial mode. In addition, the device had to collect data accurately and keep the noise in the system as low as possible concurrently. The frame was designed by CAD software and manufactured by a 3D printing machine. The copper clad laminate has a layer of copper coated on a flexible polyimide sheet. It was etched to make the electrode terminal's connection and glued to the frame using DP105 manufactured by 3M Co. Fig. 5(a) shows the exploded view of the new probe and semi-finished product is shown in Fig. 5(b).

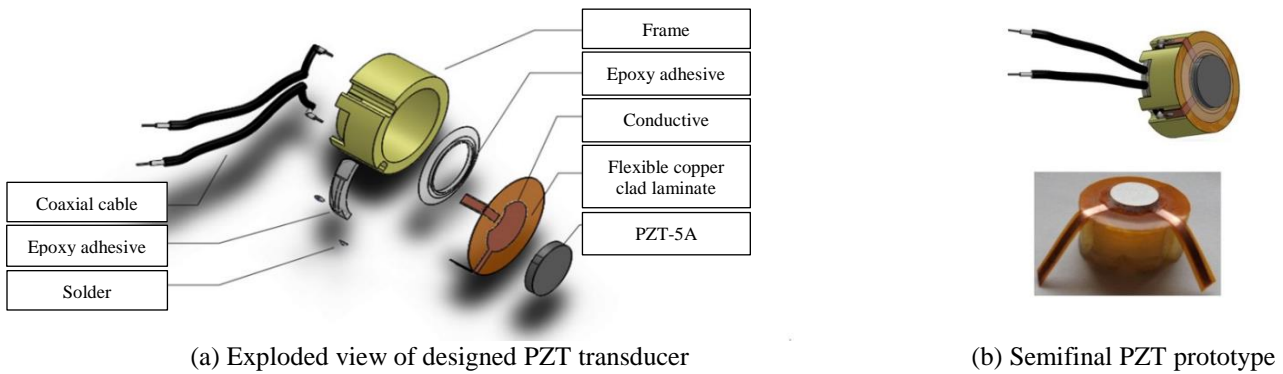


Fig. 5 PZT transducer probe

Since the polyimide sheet was flexible, it was highly possible that it would deform when PZT transducer was placed on the surface of the specimen. The deformation might in some cases impair the uniform contact between the transducer and the target surface. We used a cap to solve this issue. The polymer flexible cap improved the efficiency of the new probe by providing the back pressure. The C8 flexible cap manufactured by Ningbo Flashlight Co was used. The cap's dimension and the final assembled probe are shown in Fig. 6.



Fig. 6 Cap's dimensions and the final assembled prototype

By pressing the cap, the trapped air was compressed between the cap and polyimide sheet. The compressed air provided some back pressure on the polyimide sheet and therefore the deformation of the polyimide sheet was reduced during the experiments of Fig. 7.

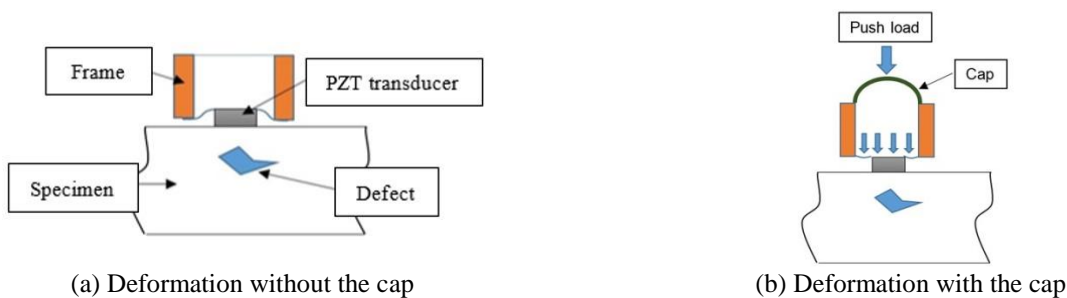


Fig. 7 Schematic view of the designed PZT transducer probe with/without back pressure on a sample specimen

Coaxial cable connected the PZT transducer to the evaluation board. The cable was manufactured by Shikoku Co. and the outer diameter was 1.8mm. It had an inner conductive core and outer braided shield. The coaxial cable has several advantages such as less electromagnetic noise because the inner core is in a Faraday shield. As less interference and crosstalk were expected to happen, we could use longer cables. The core of cable was connected to each terminal of PZT transducer and braided shield was connected to the ground terminal on the AD5933 evaluation board. The mini BNC connectors were used for connection of PZT transducer and AD5933 evaluation board. These connectors are very stable and easy to use as well. The mini BNC connectors were used for calibration of the required resistor as well. The Outer diameter of mini BNC connector was 10 mm with a length of almost 20 mm. Fig. 8(a) shows the BNC connectors and coaxial cables.

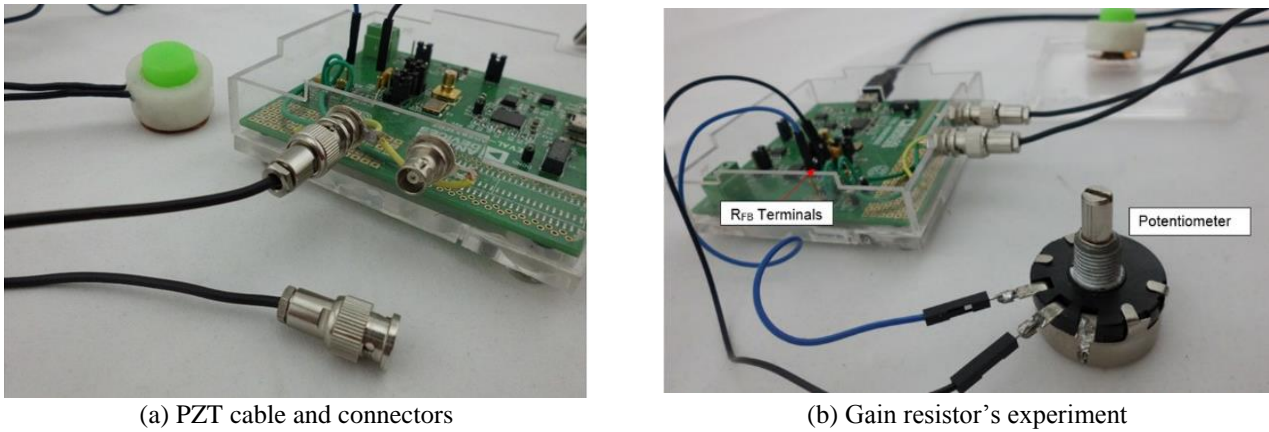


Fig. 8 PZT transducer and evaluation board

To ensure the contact between the surface of the specimen and the transducer, the probe needed to be manually pressed on the surface of the specimen, but we were wondering that what will be the threshold of the pressure without interfering the measured impedance. The applied force F_p was not easily controllable during the test from one step to another, therefore, the results will not be easily interpretable if F_p has a significant effect on the measured impedance. Coupling gel is used to maximize the contact between surfaces of the PZT transducer and specimen. The test setup included an adjustable clamp which was attached to a weight scale. The clamp has been adjusted to induce a uniform load on the surface plate of scale. The test setup is shown in Fig. 9(a) and the schematic of the experiment are shown in Fig. 9(b).

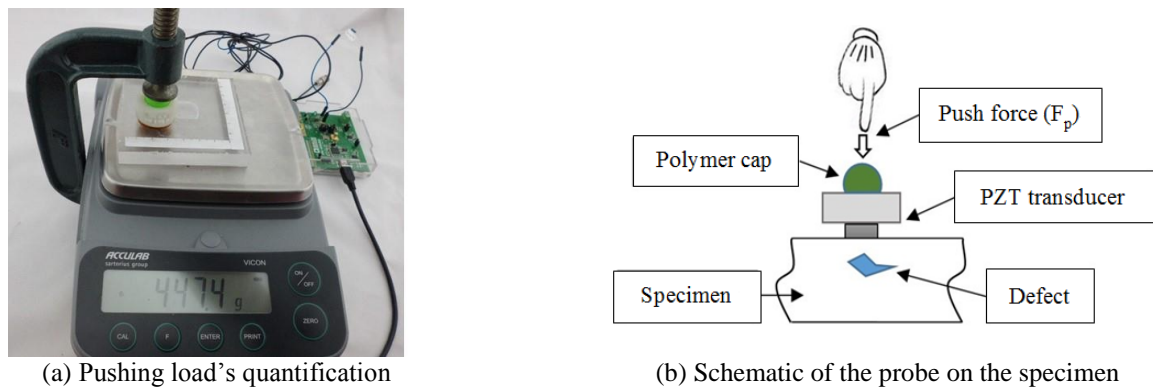


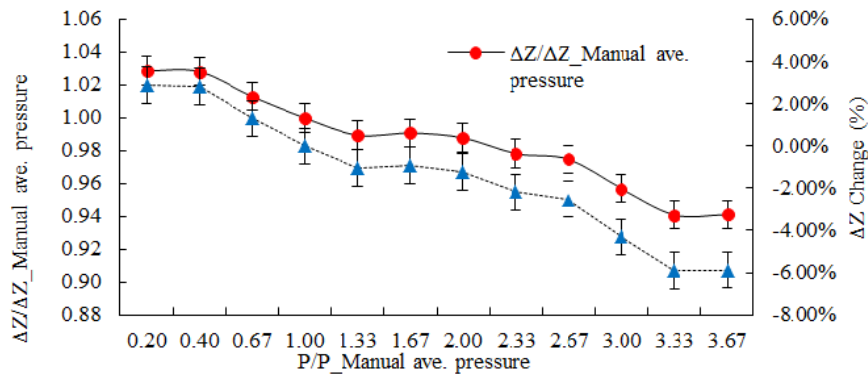
Fig. 9 Pushing experimental setup

The axial pressure on the PZT transducer was increased from zero to approximately 0.69 MPa by fastening the clamp. The freeloading case in this experiment was obtained when the PZT transducer rested on the surface of a specimen without any additional push force and just due to its weight ($m=10.3$ g) and the surface tension of the sticky coupling gel. A random specimen with a debonding defect was selected and used for this experiment. The steps of the experiment included the calibration of the system, setting the push forces and finally measuring the impedance and phase on the debonding area. These steps were repeated for each push force.

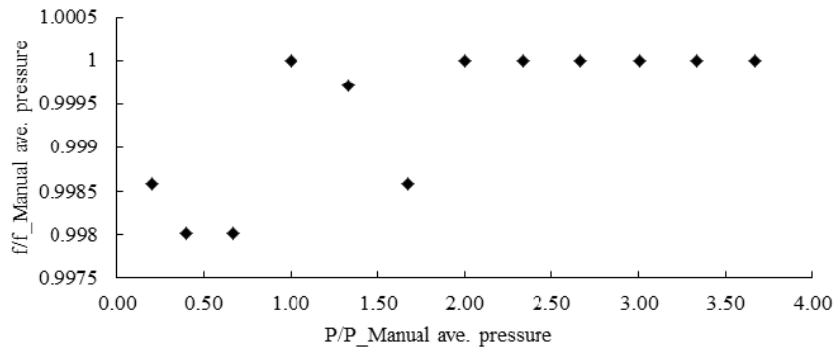
On the figure, ΔZ refers to the difference of peak impedance and fitted curve, proportional to $1/f$, as shown in Fig. 1. Using ΔZ provides a more meaningful result as its magnitude is only affected by abnormalities and damage in the structure. The normal push loads by hand have been measured on the scale several times and it has been observed that the magnitude of hand forces did not exceed more than 15N approximately, corresponding to a pressure less than 0.19 MPa on the PZT transducer. Measured impedances by several hand pressures were averaged and has been considered as the reference impedance ($\Delta Z_{\text{Manual ave. pressure}}$) and clamp measured impedance magnitudes were normalized with respect to this $\Delta Z_{\text{Manual ave. pressure}}$. It has been observed that the measured impedance decreased as the pushing force increased. In particular, the normalized impedance decreased from a value of 1.03 to 0.94 when the normalized pressure increased from

approximately 0.2 to 3.67. The impedance change was very small compared to the large change of the pressure. The results are shown in Fig. 10(a). In this figure, normalized impedance ($\Delta Z/\Delta Z_{\text{Manual ave. pressure}}$) versus normalized pressure ($P/P_{\text{Manual ave. pressure}}$) is shown which $\Delta Z_{\text{Manual ave. pressure}}$, refers to the measured impedance of average manual pushing pressure's conditions; on the same plot is also shown the impedance change percentage (ΔZ Change, %) regarding to the measured impedance of average manual pushing pressure's conditions ($\Delta Z_{\text{Manual ave. pressure}}$, 0.19 MPa), with the resonance frequency-245 kHz, PZT-5A, diameter of 10 mm and thickness of 3.7 mm. The measured impedance changed a little compared to the large change of applied pressure. Therefore, the effect of a varying push force on the measured impedance could be neglected.

Another experiment on the resonance frequency gave the same idea as the impedance experiment provided. The frequency did not shift significantly when the applied pressure was increased. However, the constant value of normalized frequency in a range of normalized pressure could be explained by the relative coarse frequency's step size. The resonance impedance was measured for each pressure condition and the frequency and phase values corresponding to resonance impedance were recorded as well. The resonance frequencies were normalized by the resonance frequency of average manual pushing pressure's conditions ($f_{\text{Manual ave. pressure}}$), Fig. 10(b).



(a) Normalized impedance versus normalized pressure



(b) Normalized resonance frequency versus normalized pressure

Fig. 10 Pushing load's experimental results

3.2. LAI transducer electronics

In this study, the AD5933 evaluation board (Analog Device Corporation) was used to measure the electromechanical response of a PZT transducer in the kHz range. AD5933 is a portable impedance analyzer that is useful for low-frequency ranges. The impedance measurement relies on calibration and comparison. The unknown impedance is connected to the external voltage terminals. The AC current passes through the Z_{unknown} (unknown impedance) and R_{FB} (external feedback resistor). If the output voltage, R_{FB} and the gain along the signal pass are known, the unknown impedance can be calculated by sampling and processing of the voltage at the output of Low Pass Filter (LPF). The board can measure the impedance by providing the real (R) and imaginary (I) part of the impedance. The magnitude is given by $\text{Magnitude}(f) = \sqrt{R^2 + I^2}$, that is

equal to a scaled value of the actual impedance at frequency point f . The actual value of impedance can be obtained by multiplying the magnitude value by a scaling factor called the gain resistor. The gain resistor is calculated during the calibration of the system with a known impedance connected to the external voltage terminals. The sweep parameters need to be set in the first step. It is important to know the approximate frequency of radial resonance mode because the program cannot sweep a wide range of frequency in each step. The sweep parameters need to be adjusted to cover at the radial resonance frequency in the range. The internal oscillator has been used for programming the setting. The calibration process uses a known resistor. However, it is possible to use a capacitor or combination of resistor-capacitor as well. The frequency range of excitation has been chosen based on specification provided by the PZT supplier, American Piezo Co. to ensure having the first radial resonance mode in the frequency range:

$$f_r = \frac{N_p}{2r} \quad (9)$$

$$f_t = \frac{N_t}{h} \quad (10)$$

where f_r , f_t , N_p , N_t , r , and h are the radial resonance frequency, the thickness resonance frequency, the radial mode frequency constant, the thickness mode frequency constant, and the transducer's radius and thickness respectively. Frequency constants of the PZT transducer were provided by the manufacturer.

The AD5933 evaluation board required calibration before any experiment. To choose the optimal gain resistor, an experiment with a variable gain resistor (i.e., potentiometer) was designed. The potentiometer's resistance range was 0-100 k Ω . The potentiometer has been connected to the board's R_{FB} terminals by short breadboard wires. The AD5933 has been connected to PC or laptop which has the AD5933 software installed already. The calibration process required a connected known impedance (for example, a precise resistor which was 50 k Ω in this experiment) to external terminals of the board and then the gain factor was calculated. After calibration, the PZT transducer has been excited and the impedance and phase magnitudes have been measured for both cases of PZT's free vibration in the air and the transducer on the specimen with a debonding defect. The aim of this experiment was the calculation of the signal to noise ratio, which provides a logical scale to choose the most proper gain resistor. The setup of the board and potentiometer are shown in Fig. 8b. The setup includes a potentiometer range 0-100 k Ω connected to R_{FB} terminals on AD5933 evaluation board, PZT-5A, the diameter of 10 mm and thickness of 3.7 mm.

Following the successful setup of the circuit, the potentiometer was adjusted for different gain resistors which the precise value of the resistor was measured by a multimeter frequently. MATLAB functions are used to filter the noise in the measured impedance and phase magnitudes. The aim of the MATLAB code was the approximate calculation of signal to noise ratio. The impedance data were smoothed by the Local Regression Smoothing method that the data were modeled locally by the polynomial weighted least squares regression. MATLAB function is "smooth (Y, Span, Method)", which "Y" is the sampled data, "Span" defines a window of neighboring points to include in the smoothing calculation for each data point. A larger span increases the smoothness but decreases the resolution of the smoothed data set. The selected smoothing method provides the fittest curves to measured noisy impedance data.

The noisy sampled and smoothed impedance data were processed by the MATLAB program. The smoothed data have been considered as a reference and the deviation of sampled data from smoothed data has been calculated and defined as the approximate error's value. The signal to noise percentages for all points of data was calculated:

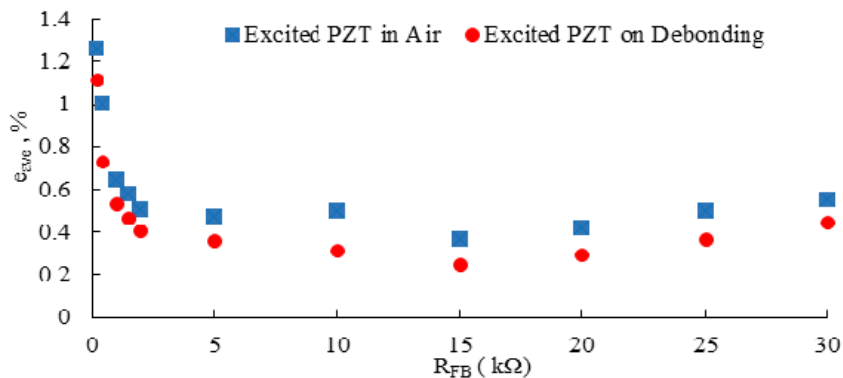
$$e_i \% = \left| \frac{NI_i - SI_i}{NI_i} \right| \times 100 \quad (11)$$

Finally, the average of percentages has been calculated for all n points of sampling as follows:

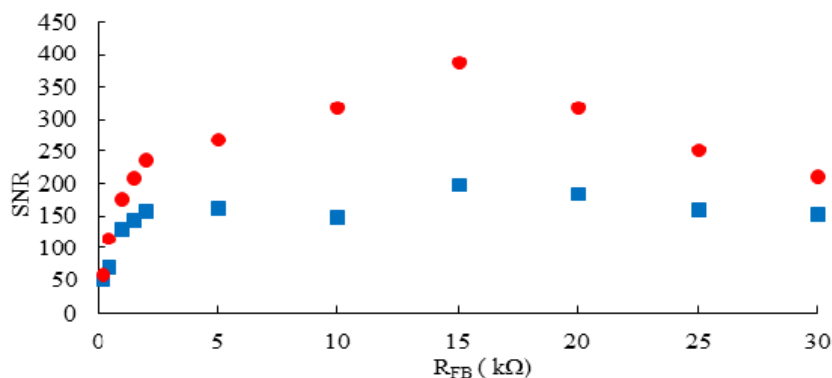
$$e_{ave} \% = \frac{\sum_{i=1}^n e_i \%}{n} \tag{12}$$

The average value of noise was calculated for each gain resistor test in two scenarios. First, the PZT transducer was excited freely at air and then the PZT transducer has been tested on debonding defect in the second scenario. The real experiment was simulated to check the validity of results in the case of real boundary conditions. It is possible that defect may introduce extra noise into the system, therefore it has been tried to keep the same testing conditions for the debonding case. Impedance was measured just for one location at the center of the defect’s region for all gain resistors.

Based on the experimental results, the gain resistors higher than 50 kΩ and very low resistors close to zero do not register any impedance peak by this setup. The experiment proved that the proper gain resistor range was 10-20 kΩ, where the mean noise percentage is minimum, Fig. 11 (a). The noise percentage raised to 20% in some frequencies, but the average value of noise remained less than 2% in all cases. The noise percentage technique was not the precise method in resistor’s selection, but it was a reliable approximate method to choose the proper gain resistor. The ideal gain resistor range is 10-20 kΩ which the signal to noise ratio, SNR, is maximum in this range. Fig. 11 (b) shows that SNR was increasing significantly in responding to the proper gain resistor. Despite fewer noise deviations in higher gain resistors, the measured impedance magnitude showed that the lower gain resistors produce higher measured impedance magnitude, therefore the optimized gain resistor has been set as 10 kΩ in this study, which was in a proper gain resistor range and produced higher measured impedance magnitude. In the figure, average signal to noise percentage (e_{ave}) versus the gain resistor value (R_{FB}) is shown with the resonance frequency of 245 kHz, tested by an AD5933 evaluation board, PZT-5A, diameter of 10 mm and thickness of 3.7 mm. It also shows the signal to noise ratio, SNR, versus the gain resistor value (R_{FB}), which shows the effect of different gain resistors on noisy measured radial resonance impedance.



(a) Average signal to noise percentage versus the gain resistor value



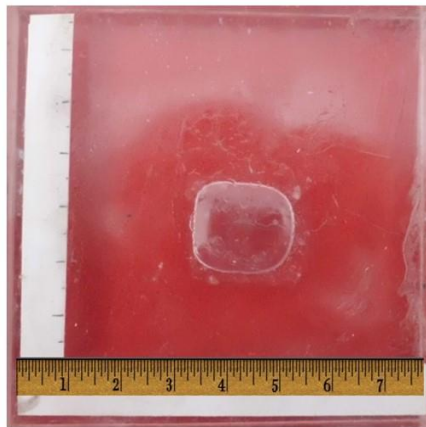
(b) Signal to noise ratio versus the gain resistor value

Fig. 11 Optimal gain’s experimental results (continued)

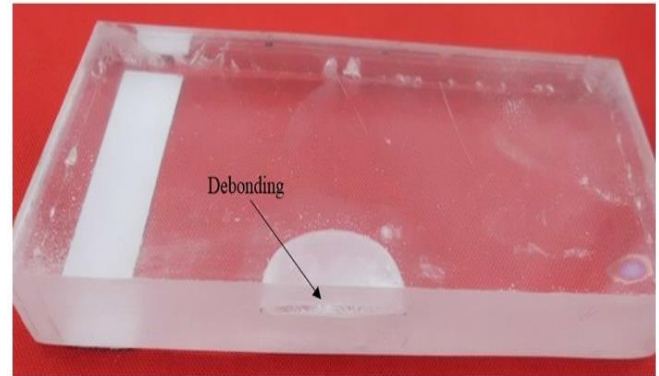
4. Transducer Validation

4.1. Experimental validation

The setup was evaluated for the debonding as a common defect. Two plates of PMMA have been cut and stacked on by regular epoxy glue through the vacuum bagging process. The debonding was simulated by sanding both surfaces in a small region. The size of the specimen was 80*80 mm which was combined from two plates with different thickness. The thickness of the first plate was 8 mm and the other one was 3 mm. The size of the debonding area is 20*17*2 mm approximately. The specimen is shown in Fig. 12(a) with the cross-section in Fig. 12(b). The resonance frequency of the PZT transducer was 245 kHz, tested by AD5933, PZT-5A, the diameter of 10 mm and a thickness of 3.7 mm.

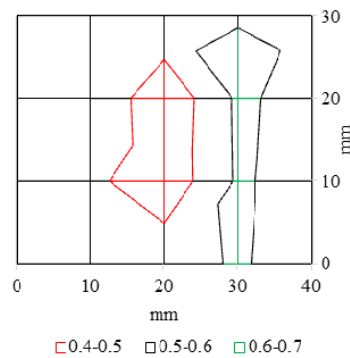


(a) Geometry of debonding

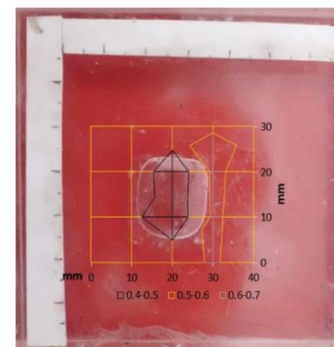


(b) Cross-section of debonding

Fig. 12 PMMA specimen with debonding



(a) Contour plot of normalized impedance



(b) Superimposition of contour plot

Fig. 13 Superimposition of measured impedance on debonding

The surface was gridded in four rows and five columns with a step size of 10 mm. The impedance values were normalized by the impedance of the transducer's resonating without any load in the air. The 2D contour surface plot of normalized impedance for the thin side (3 mm) is shown in Fig. 13(a). The red region shows the debonding area. The measured impedance on the debonding region was smaller than in other locations. The top sheet size was 80*80*3 mm and bottom sheet size was 80*80*8 mm, they were glued by an epoxy adhesive through the vacuum bagging process. The normalized impedance, $\Delta Z/\Delta Z_0$, on the debonding region is shown in red with a range of 0.4-0.5, non-defected regions with the $\Delta Z/\Delta Z_0$ in a range of 0.6-0.7 is shown in black and a side region with the $\Delta Z/\Delta Z_0$ in a range of 0.5-0.6 is shown in green which might be a result of some trapped air during the gluing process. As a comparison, the average of normalized impedance over the non-defected regions was 0.55 which decreased by 18% on the debonding to an average of 0.45. Since we used liquid glue to attach two layers of the specimen, the debonding cavity was filled with the glue and it could be the reason for the decreased impedance. In regard to side region with a higher normalized impedance which is shown in green in Fig. 13(a), the normalized impedance

increased by 18% as well. LAI technique could detect the presence of abnormalities successfully, but it did not provide any information about the depth or severity of defects. With the coarse step size of 10 mm, just two measuring spots were located on the debonding region which was not enough to estimate the geometry of defect. However, the length of the defect along the y-axis was matched to the geometry of debonding.

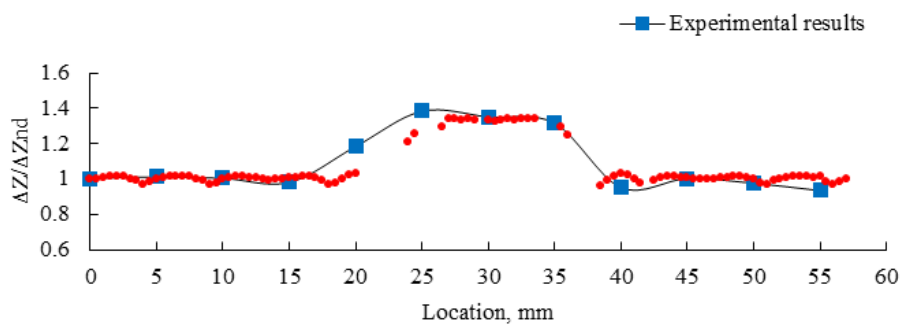
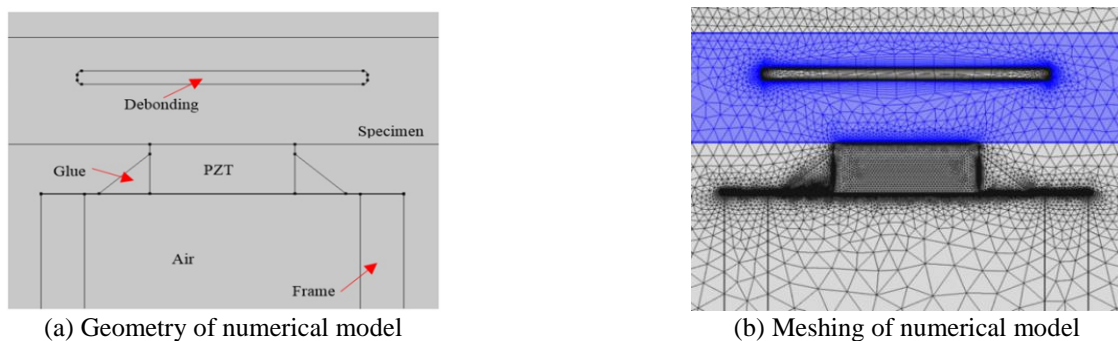
The superposition of the measured impedance results and the specimen is shown in Fig. 13(b) as well. The debonding region was matched in both measured impedance and visual test of the specimen. LAI technique clearly showed its ability to detect this type of defects. At column 30 mm, some trapped air bulbs were visible, which measured impedance could detect it as well. Therefore, the contour plot had three regions including well glued, debonding and trapped air regions.

4.2. Experimental validation

Table 1 Material properties

	Transducer (PZT-5A)	Specimen (PMMA)	Frame (ABS)	Flexible clad laminate (Polyimide)	Glue (Epoxy resin)
Density (kg/m ³)	7750	1190	1030	1300	1100
Speed of sound (m/s)	4350	2270	2230	2200	2400

The 2D numerical model of debonding was created by COMSOL Multiphysics v5.0 software. The geometry of debonding including PZT transducer, specimen, and surrounding air are shown in Fig. 14. In order to simulate the PZT transducer and specimen interactions, we used the Acoustic-Piezoelectric Interaction module in the frequency domain. As a boundary condition, the PZT transducer was fully coupled to the specimen using acoustic-structure boundary condition. Since the boundary conditions employed the full coupling of the PZT transducer and specimen, the thin layer of coupling gel was eliminated in the numerical model. We also assumed that the thickness of the coupling gel layer was negligible after moderate pushing of the transducer on the smooth surface of the specimen. Since LAI technique relies on changes in the acoustic impedance, the main material properties that were used in the numerical simulations were the density of materials and speed of sound in different domains. COMSOL library of materials and previous literature, mentioned in the introduction, where the resources of Table 1. Other material properties of PZT-5A including the elasticity and coupling matrices, in addition to the relative permittivity, were automatically added by the COMSOL material library.



(c) Numerical versus experimental results

Fig. 14 Normalized simulation

The PZT transducer moved on the surface of the specimen and collected the impedance point by point. The step size of movement was 0.5 mm which was accurate enough for the numerical modeling. The assigned materials were like the experiment of debonding as PMMA, PZT transducer, glue, and trapped air. The main required material specifications in the numerical modeling were density and speed of sound. The mesh elements' sizes are relatively several magnitudes smaller than the wavelength of PZT transducer. The sweeping frequency was 100-250 kHz. The maximum and minimum element sizes were 0.2 mm and 4.0E-4 mm with a curvature factor of 0.2 which provided an extremely fine mesh. The numerical solver used the PARDISO method. The calculated impedance values were normalized by the average of calculated impedances in four locations far from the debonding (ΔZ_{nd}). The numerical versus experimental results are shown in Fig. 14.

PMMA specimen with the debonding depth of 5 mm was tested by the PZT-5A transducer with the resonance frequency of 245 kHz, using AD5933, and transducer's diameter of 10 mm and thickness of 3.7 mm. The numerical model was done by the COMSOL Multiphysics. The calculated and measured impedance showed an increase of around 35% when the PZT transducer arrived on the debonding area in both experimental and numerical approaches. The numerical results showed a good agreement with the experimental results which validated the efficacy of LAI technique in the detection of near-surface defects like debonding.

5. Conclusions

A novel cost-effective and efficient LAI technique has been introduced in this study. This technique was able to detect the abnormalities and defects in LAI structures. The fundamental and physical principle of the technique relies on monitoring the energy transmission between a resonating transducer and a target surface. Briefly, the impedance signatures at different locations of the structure were measured and the presence of abnormalities was inferred by their effect on the measured impedance. For this purpose, setup elements including hardware and software were designed and developed. In addition, the validity of the technique has been verified by different experiments and numerical models. After ensuring the stability of setup, different experiments have been run to validate the proficiency of LAI technique. The resonance frequency of the PZT transducer was 245 kHz working at the radial resonance mode. It was shown that varying manual pushing pressure on the transducer changed the normalized measured impedance from 1.03 to 0.94 which was neglectable. The proper gain resistor was measured as 10 k Ω to minimize the noise and mismatching. The Experimental evaluation could detect the debonding at a depth of 3 mm and could approximate the geometry of defect.

The numerical model of debonding has been developed as well and both experimental and numerical results showed very good agreement with an increase of around 35% on the debonding area. The future work includes running more experiments to evaluate the efficacy of this method on the detection of abnormalities and defects in different materials like polymer composites, wooden structures, and biomedical applications. However, technical optimization of the current setup in terms of accuracy and efficacy could be another target. The evaluation board has some unnecessary components that can be removed, and the board could be more compact. These developments could make the LAI setup very compact and easy to use for more regular daily applications. Because of LAI nature of biological structures, the biomedical application remains a very potential field for further investigations. This research received no specific grant from any funding agency in the public, commercial, or not-for-profit sectors.

Acknowledgement

We would like to express our gratitude to Prof. Yaping Dan (UM-SJTU JI), Prof. Yu Zhefeng (School of Aeronautics and Astronautics, SJTU) and Prof. Aili Zhang (School of Biomedical Engineering, SJTU), Mr. Rui Zhang (UM-SJTU JI), Mr. Baojun Ning (School of Aeronautics and Astronautics, SJTU) and Mr. Sun Bin (Micro-Nano Key Institute, SJTU) for their

support and contribution on setting up and experimental issues. This paper was a part of master's thesis in Mechanical Engineering at the University of Michigan – Shanghai Jiao Tong University Joint Institute.

Conflicts of Interest

The authors declare that there is no conflict of interest.

References

- [1] C. R. Farrar and K. Worden, "An introduction to structural health monitoring," *Philosophical Transactions of the Royal Society a-Mathematical Physical and Engineering Sciences*, Editorial Material vol. 365, no. 1851, pp. 303-315, February 2007.
- [2] C. R. Farrar and N. A. J. Lieven, "Damage prognosis: the future of structural health monitoring," *Philosophical Transactions of the Royal Society a-Mathematical Physical and Engineering Sciences*, Article vol. 365, no. 1851, pp. 623-632, February 2007.
- [3] H. Salehi and R. Burgueno, "Emerging artificial intelligence methods in structural engineering," *Engineering Structures*, Review vol. 171, pp. 170-189, September 2018.
- [4] S. Sony, S. Laventure, and A. Sadhu, "A literature review of next-generation smart sensing technology in structural health monitoring," *Structural Control & Health Monitoring*, Review vol. 26, no. 3, p. 22, March 2019.
- [5] S. Nezami, S. Lee, K. Kang, and J. Kim, "Improving durability of a vibration energy harvester using structural design optimization," no. 50497, p. V002T07A018, September 2016.
- [6] S. Nezami, H. Jung, M. K. Sung, and S. Lee, "Dynamics of vibration energy harvester governed by gravity and magnetic force in a rotating wind turbine blade," no. 51951, p. V002T07A002, September 2018.
- [7] B. S. Divsholi and Y. W. Yang, "Combined embedded and surface-bonded piezoelectric transducers for monitoring of concrete structures," *Ndt & E International*, Article vol. 65, pp. 28-34, July 2014.
- [8] W. S. Na and J. Baek, "A review of the piezoelectric electromechanical impedance based structural health monitoring technique for engineering structures," *Sensors*, Review vol. 18, no. 5, p. 18, May 2018.
- [9] F. G. Baptista, J. Vieira, and D. J. Inman, "Sizing PZT transducers in impedance-based structural health monitoring," *Ieee Sensors Journal*, Article vol. 11, no. 6, pp. 1405-1414, June 2011.
- [10] K. S. Tan, N. Guo, B. S. Wong, and C. G. Tui, "Comparison of lamb waves and pulse echo in detection of near-surface defects in laminate plates," *NDT & E International*, vol. 28, no. 4, pp. 215-223, August 1995.
- [11] E. La Malfa Ribolla, M. R. Hajidehi, P. Rizzo, G. F. Scimemi, A. Spada, and G. Giambanco, "Ultrasonic inspection for the detection of debonding in CFRP-reinforced concrete," *Structure and Infrastructure Engineering*, Article vol. 14, no. 6, pp. 807-816, 2018.
- [12] R. Dugnani, "Novel nondestructive evaluation transducer for imaging of low-impedance targets," *Journal of Intelligent Material Systems and Structures*, Article vol. 26, no. 3, pp. 340-351, February 2015.
- [13] D. M. Ai, H. P. Zhu, H. Luo, and C. Wang, "Mechanical impedance based embedded piezoelectric transducer for reinforced concrete structural impact damage detection: A comparative study," *Construction and Building Materials*, Article vol. 165, pp. 472-483, March 2018.
- [14] A. Narayanan, A. Kocherla, and K. V. L. Subramaniam, "Embedded PZT sensor for monitoring mechanical impedance of hydrating cementitious materials," *Journal of Nondestructive Evaluation*, Article vol. 36, no. 4, p. 13, December 2017.
- [15] H. A. Tinoco, L. Robledo-Callejas, D. J. Marulanda, and A. L. Serpa, "Damage detection in plates using the electromechanical impedance technique based on decoupled measurements of piezoelectric transducers," *Journal of Sound and Vibration*, Article vol. 384, pp. 146-162, December 2016.
- [16] R. Dugnani, "Novel transducer for characterization of low-impedance materials," presented at the Proceedings 4th Asia-Pacific Workshop on SHM, December, 2012.
- [17] Elcometer, "<http://www.elcometerusa.com/ultrasonic-ndt/Flaw-Detectors>," ed, 2019.
- [18] S. Kim et al., "Health monitoring of civil infrastructures using wireless sensor networks," presented at the Proceedings of the 6th international conference on Information processing in sensor networks, Cambridge, Massachusetts, USA, 2007.
- [19] P. Gyuhae, S. Hoon, C. R. Farrar, and D. J. Inman, "Overview of piezoelectric impedance-based health monitoring and path forward," *Shock and Vibration Digest*, vol. 35, no. 6, pp. 451-463, 2003.
- [20] R. Dugnani and F. K. Chang, "In vitro atherosclerotic plaque characterization by acoustic impedance monitoring, Part II: Experimentation and validation," *Journal of Intelligent Material Systems and Structures*, Article vol. 19, no. 7, pp. 827-835, July 2008.

- [21] A. Mohammadabadi and R. Dugnani, "Wood defect detection using low acoustic impedance-based PZT transducers," *engrXiv*, 2019.
- [22] N. Kim, K. Jang, and Y. K. An, "Self-sensing nonlinear ultrasonic fatigue crack detection under temperature variation," *Sensors*, Article vol. 18, no. 8, p. 15, August 2018.
- [23] A. Mohammadabadi and R. Dugnani, "Damage detection in composites by LAI-PZT transducer," *engrXiv*, 2019.
- [24] K. Oshima, T. Takigami, and Y. Hayakawa, "Robust vibration control of a cantilever beam using self-sensing actuator," *JSME International Journal, Series C (Mechanical Systems, Machine Elements and Manufacturing)*, vol. 40, no. 4, pp. 681-687, 1997.
- [25] M. Rakotondrabe, I. A. Ivan, S. Khadraoui, P. Lutz, and N. Chaillet, "Simultaneous displacement/force self-sensing in piezoelectric actuators and applications to robust control," *IEEE/ASME Transactions on Mechatronics*, vol. 20, no. 2, pp. 519-531, 2015.
- [26] R. Dugnani and F. K. Chang, "In vitro atherosclerotic plaque characterization by acoustic impedance monitoring, Part I: Sensor modeling, design, and fabrication," *Journal of Intelligent Material Systems and Structures*, Article vol. 19, no. 7, pp. 815-826, July 2008.
- [27] R. Dugnani, "Dynamic behavior of structure-mounted disk-shape piezoelectric sensors including the adhesive layer," *Journal of Intelligent Material Systems and Structures*, Article vol. 20, no. 13, pp. 1553-1564, September 2009.
- [28] C. Liang, F. P. Sun, and C. A. Rogers, "Coupled electro-mechanical analysis of adaptive material systems-determination of the actuator power consumption and system energy transfer," *Journal of Intelligent Material Systems and Structures*, vol. 5, no. 1, pp. 12-20, January 1994.
- [29] L. Chen, S. Fanping, and C. A. Rogers, "Electro-mechanical impedance modeling of active material systems," *Smart Materials and Structures*, vol. 5, no. 2, pp. 171-186, April 1996.
- [30] J. Shen and S. Mousavi, "Least sparsity of ℓ_1 -norm based optimization problems with ℓ_2 regularization," *SIAM Journal on Optimization*, vol. 28, no. 3, pp. 2721-2751, 2018.
- [31] V. Gupta, M. Sharma, and N. Thakur, "Optimization criteria for optimal placement of piezoelectric sensors and actuators on a smart structure: A technical review," *Journal of Intelligent Material Systems and Structures*, Review vol. 21, no. 12, pp. 1227-1243, August 2010.
- [32] N. Pérez, F. Buiocchi, M. A. Brizzotti Andrade, and J. C. Adamowski, "Numerical characterization of piezoceramics using resonance curves," *Materials (Basel, Switzerland)*, vol. 9, no. 2, p. 71, 2016.



Copyright© by the authors. Licensee TAETI, Taiwan. This article is an open access article distributed under the terms and conditions of the Creative Commons Attribution (CC BY-NC) license (<https://creativecommons.org/licenses/by-nc/4.0/>).